ORGANOMETALLICS

Article

pubs.acs.org/Organometallics

Synthesis of Oxorhenium Acetyl and Benzoyl Complexes Incorporating Diamidopyridine Ligands: Implications for the Mechanism of CO Insertion

Cassandra P. Lilly, Paul D. Boyle, and Elon A. Ison*

Department of Chemistry, North Carolina State University, 2620 Yarbrough Drive, Raleigh, North Carolina 27695-8204, United States

Supporting Information

ABSTRACT: A series of oxorhenium alkyl, phenyl, and vinyl complexes of the form [(DAP)Re(O)(R)] (R = aryl, vinyl, alkyl) was reported, and their reactivity with CO was examined. The methyl complex **5a** reacts with CO at a significantly faster rate (2.5 h) than the phenyl complex **7a** (24 h). Computational (B3PW91) studies reveal that although the acyl complex is the least stable (ΔG_{353} = −11.2 kcal/mol) with respect to CO insertion compared to the benzoyl complex (ΔG_{353} = −14.5 kcal/mol), the activation energy for CO insertion is lower for the methyl complex ($\Delta G^{\ddagger}_{353}$ = 14.6 kcal/mol) than for the phenyl complex ($\Delta G^{\ddagger}_{353}$ = 17.4 kcal/mol). This is consistent with the previously proposed mechanism, where CO inserts directly into the Re−R bond without prior formation of a CO adduct. The X-ray crystal structures of complexes **6**, **7a**, **8a**, and **9a** are reported.

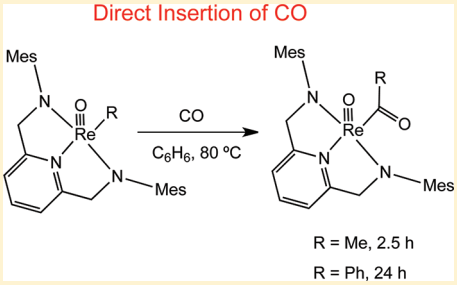

INTRODUCTION

Acyl complexes have been proposed as intermediates in many important catalytic reactions, including acetic acid synthesis,[1] hydroformylation,[2] and hydroacylation reactions.[3] However, for these systems, the acyl ligands are often incorporated into complexes where the metal is in a low oxidation state.[4] The reaction between [(DAAm)Re(O)(CH_3)] (**1**; DAAm = *N*,*N*-bis(2-arylaminoethyl)methylamine; aryl = C_6F_5, Mes) and CO, to form the rhenium(III) acetate complex [(DAAm)Re(O_2CCH_3)(CO)] (**2**) was previously reported (Scheme 1).[5]

Scheme 1

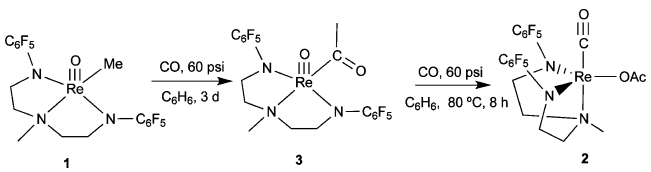

It was shown the reaction proceeds by direct insertion of CO into the Re−Me bond in **1**, without prior formation of a CO adduct, to produce an oxorhenium acyl intermediate, [(DAAm)Re(Ac)] (**3**). This is followed by 1,2-migration of the acyl ligand to the terminal oxo, in the presence of CO, to generate **2**.

Complex **3** is a rare example of a high-oxidation-state (Re^{V}) acyl complex, incorporating an oxo ligand,[6] and unlike acyl complexes incorporating low-valent metals, very little is known about the reactivity of high-valent metal acyls. The incorporation of strongly π donating oxo ligands and π accepting acyl ligands may lead to enhanced reactivity.[7] Thus, a systematic study of the synthesis and reactivity of these complexes is warranted.

In addition to the previous work with the DAAm ligands, we have also reported the synthesis of related complexes incorporating diamidopyridine (DAP = 2,6-bis((mesitylamino)-methyl)pyridine) pincer ligands.[8] These complexes exhibit reactivity similar to that of the DAAm complexes, but their rigid structure leads to greater stability and increased reactivity in catalytic reactions. The pyridine backbone of the DAP pincer ligands also allows for the ability to tune the electronics at the metal center by incorporating substituents in the para position of the pyridine ring, as outlined in Scheme 2.

Scheme 2

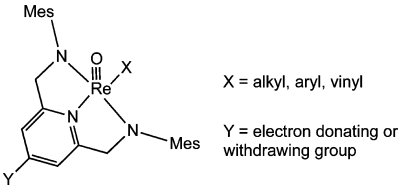

In this paper, the syntheses of several new oxorhenium alkyl, phenyl, and vinyl complexes of the form [(DAP)Re(O)(R)] (R = aryl, vinyl, alkyl) are reported, and their reactivity with CO is examined. Insights into the mechanism of CO insertion into Re−R bonds were attained from these studies. In addition, computational (DFT) studies were utilized in order to

Received: April 9, 2012
Published: May 25, 2012

   dx.doi.org/10.1021/om3002872 | *Organometallics* 2012, 31, 4295−4301

understand the differences in reactivity with CO for alkyl, vinyl, and aryl complexes incorporating DAP ligands.

RESULTS AND DISCUSSION

Synthesis of [(DAP)Re(O)(R)] Complexes. The chloride complexes **4** were synthesized by treatment of the DAP ligand with $Re(O)Cl_3(PPh_3)_2$, as previously reported.[8] In the case of complex **4b**, the ligand 2,6-bis((mesitylamino)methyl)-4-methoxypyridine, which features a methoxy group in the para position of the pyridine backbone, was utilized. This ligand was synthesized by the reaction of 2,6-dibromomethyl-4-methoxypyridine[9] with 2 equiv of LiNHMes.

Oxorhenium alkyl, aryl, and vinyl complexes (**5**–**7**) were synthesized by transmetalation from the corresponding Grignard reagents according to Scheme 3. The original synthesis of the oxorhenium methyl complex **5a** involved treatment of the DAP ligand with PPh_3 and methyltrioxorhenium (MTO).[8] However, this synthesis results in the generation of 1 equiv of $OPPh_3$ as a byproduct, which is difficult to separate from **5a**. Thus, the transmetalation strategy represents an improved synthesis, as it avoids the generation of this byproduct. Complex **5b**, which features a methoxy group in the para position of the pyridine backbone of the DAP ligand, was also synthesized as a pink powder in 72% yield by this method.

Scheme 3

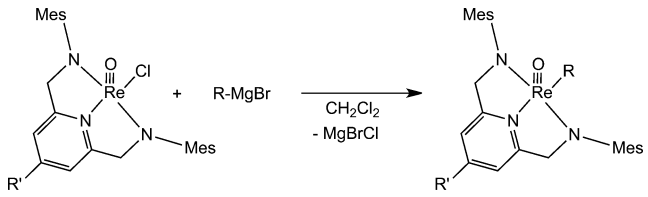

The oxorhenium vinyl (**6**) and aryl complexes (**7**) were also synthesized by this method. The ^1H NMR spectrum of **6** displays a resonance at 6.67 ppm for $Re-C-H_\alpha$, which is similar to the case for the rhenium vinyl complex, $CpRe(NO)(PPh_3)(CH{=}C(CH_3)_2)$, isolated by Gladysz and co-workers, in which H_α resonates at 7.14 ppm.[10] Complex **6** is not very stable in solution. When **6** is monitored by ^1H NMR spectroscopy in CD_2Cl_2, complex decomposition is observed after 1 h. Decomposition was also observed when **6** was heated in C_6D_6 at 80 °C for 1 h. However, **6** is stable for up to 10 days in benzene at room temperature.

X-ray Crystal Structures. X-ray-quality crystals of **6** and **7a** were obtained by slow diffusion of pentane into a concentrated solution of the corresponding complex in dichloromethane at room temperature (Figures 1 and 2). The vinyl ligand in **6** is bound in an η^1 fashion (Figure 1). The Re–C bond lengths in **6** (2.094(3) Å), and **7a** (2.077(2) Å) are shorter than the sp^3 carbon–Re bond in **5a** (2.1278(17) Å).[8] For both structures the coordination sphere around the rhenium atom can best be described as distorted square pyramidal, with the oxo ligand occupying an apical position. The Re–oxo bond length for both structures is typical for triply bonded rhenium oxos.

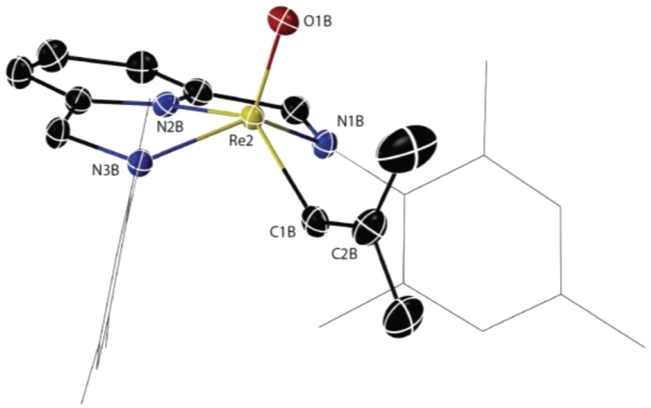

Figure 1. X-ray crystal structure of **6**. Ellipsoids are shown at the 50% probability level. Hydrogen atoms are omitted, and the mesityl substituents on the diamido ligand are depicted in wireframe for clarity. Selected bond lengths (Å) and bond angles (deg): Re2–O1B, 1.7010(19); Re2–N1B, 1.968(2); Re2–N3B, 1.973(2); Re2–N2B, 2.057(3); Re2–C1B, 2.094(3); N1B–Re2–N2B, 76.10(8); N3B–Re2–N2B, 76.11(8); O1B–Re2–C1B, 108.02(10); N1B–Re2–C1B, 88.30(9); N3B–Re2–C1B, 87.52(9); N2B–Re2–C1B, 136.35(11); O1B–Re2–N3B, 111.73(9); O1B–Re2–N1B, 112.37(9); N3B–Re2–N1B, 134.83(9); O1B–Re2–N2B, 116.28(9).

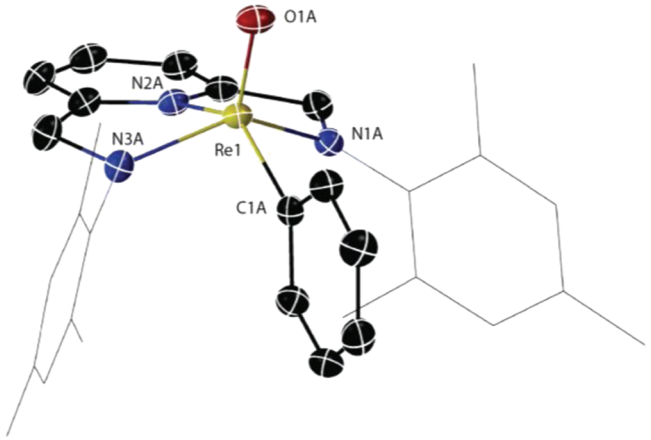

Figure 2. X-ray crystal structure of **7a**. Ellipsoids are shown at the 50% probability level. Hydrogen atoms are omitted, and the mesityl substituents on the diamido ligand are depicted in wireframe for clarity. Selected bond lengths (Å) and bond angles (deg): Re1–O1A, 1.6956(16); Re1–N1A, 1.9677(17); Re1–N3A, 1.9726(18); Re1–N2A, 2.0678(18); Re1–C1A, 2.077(2); O1A–Re1–N1A, 113.24(7); O1A–Re1-N3A, 113.13(7); N1A–Re1–N3A, 132.44(7); O1A–Re1–N2A, 114.83(7); N1A–Re1–N2A, 75.81(7); N3A–Re1–N2A, 75.90(7); O1A–Re1–C1A, 103.13(8); N1A–Re1–C1A, 90.25(7); N3A–Re1–C1A, 89.23(7); N2A–Re1–C1A, 142.04(8).

Synthesis of Acetyl and Benzoyl Complexes. DFT calculations for the migratory insertion of CO into **1** suggest that the rate-determining step for the insertion of CO into the Re–Me bond is the addition of CO to the Re complex.[5b] Thus, the rate of insertion may be influenced in these systems by changing the electron density at the metal center. This may be achieved by altering the ancillary diamido ligand. Since CO addition is rate-determining, the electronic character of the migrating R group should have a minimal effect on the rate of insertion of CO. In order to investigate the factors that affect CO insertion in the corresponding DAP complexes, the reaction of complexes **5** and **7** with CO was examined.

dx.doi.org/10.1021/om3002872 | *Organometallics* 2012, 31, 4295–4301

The reaction of **5** and **7** with CO (60 psi, C_6D_6, 80 °C) was monitored over time by ^{1}H NMR spectroscopy (see Figure S1 in the Supporting Information). These experiments allowed for a comparison of the rates of insertion into the Re−CH_3 bond versus the Re−Ar bond. Unfortunately, similar comparisons with the vinyl complex **6** were not possible, because complex **6** decomposes upon heating in C_6D_6. As shown in Scheme 4, the reaction of **5** with CO results in the formation of **8** in 2.5 h. Interestingly, altering the electronics in the para position of the pyridine backbone as in **5b** apparently has no effect on the rate of insertion, as the formation of **8b** also occurs in 2.5 h. In contrast, the formation of **9** from aryl complexes **7** requires 24 h. These data suggest that CO inserts more readily into alkyl bonds than aryl bonds.

Scheme 4

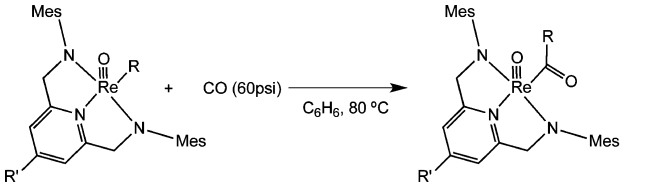

R' = H, **5a**; R' = OMe, **5b**;
R = Ph, R' = H, **7a**;
R = 4-OMePh, R' = H, **7b**;
R = 4-ClPh, R' = H, **7c**

R = Me; R' = H, **8a**, 2.5 h
R = Me; R' = OMe,**8b**, 2.5 h
R = Ph; R' = H, **9a**, 24 h
R = 4-OMePh; R' = H, **9b**, 24 h
R = 4-ClPh; R' = H, **9c**, 24 h

The migratory aptitude of the aryl ligand was also examined by changing the electronics of the aryl ligand by incorporating substituents in the para position of the phenyl ring. As shown in Scheme 4, changing the electronic nature of the aryl ligand has no effect on the rate of insertion of CO.

Thus, it appears that insertion of CO is governed by the nature of the Re−R bond. In order to investigate the difference in reactivity further, DFT calculations were performed (vide infra).

X-ray Structures of Acyl and Benzoyl Complexes. X-ray-quality crystals of **8a** were obtained by slow diffusion of pentane into a concentrated solution of **8a** in dichloromethane (Figure 3). The geometry about the metal center can best be described as distorted square pyramidal with the oxo in the apical position. The acyl oxo is positioned anti to the Re−O bond, similar to that of its DAAm analogue;[5a] the Re−C bond length decreases from 2.1278(17) Å in **3** to 2.039(4) Å. This can be attributed to the change from an sp^3 to an sp^2 carbon center along with π back-bonding from the metal center into the acyl π^* orbital. The IR stretching frequency of the C(O)−Me bond in **8a** is 1599 cm^{-1}. Bergman and co-workers report an IR stretching frequency of 1630 cm^{-1} for the acyl complex $[CpRe(CO)_2(COCH_3)(CH_3)]$,[11] while Gladysz and co-workers report an IR stretching frequency of 1545 cm^{-1} for the complex $[CpRe(NO)(PPh_3)(COCH_3)]$.[4b] These differences can be attributed to contributions from the two resonance forms depicted in Scheme 5. The alkylidene resonance form **B** is the major contributor to the bonding in complex **8a** and $[CpRe(NO)(PPh_3)(COCH_3)]$, while the acyl resonance form **A** is the major resonance contributor in $[CpRe(CO)_2(COCH_3)(CH_3)]$.[10]

X-ray-quality crystals of **9a** were also obtained by slow diffusion of pentane into a concentrated solution of **9a** in dichloromethane (Figure 4). To our knowledge, this is the first example of an oxobenzoyl complex. As in **8a**, the geometry about the metal center is best described as distorted square pyramidal, with the oxo ligand occupying the apical position. The benzoyl oxo is anti with respect to the Re−O bond. The Re−$C_{benzoyl}$ bond length is 2.059(6) Å, which is comparable to the Re−C bond length in **7a** (2.077(2) Å). The C1A−O2A bond length is 1.231(7) Å and is analogous to the C27−O2 bond length (1.224(4) Å) in **8a**.

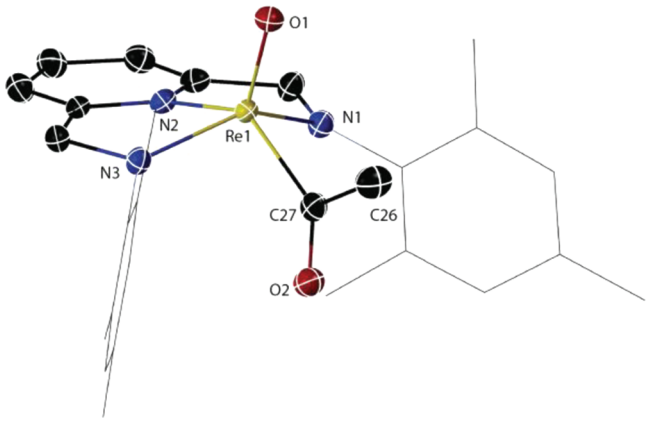

Figure 3. X-ray crystal structure of **8a**. Ellipsoids are shown at the 50% probability level. Hydrogen atoms are omitted, and the mesityl substituents on the diamido ligand are depicted in wireframe for clarity. Selected bond lengths (Å) and bond angles (deg): Re1−O1, 1.700(2); Re1−N1, 1.971(3); Re1−N2, 2.059(3); Re−N3, 1.967(3); Re1−C27, 2.039(4); O1−Re1−N3, 110.78(12); O1−Re1−N1, 109.97(11); N3−Re1−N1, 137.92(11); O1−Re1−N2, 106.45(13); N3−Re1−N2, 76.25(12); N1−Re1−N2, 76.48(11); O1−Re1−C27, 106.45(13); N3−Re1−C27, 88.78(12); N1−Re1−C27, 89.54(13); N2−Re1−C27, 136.62(12).

Scheme 5

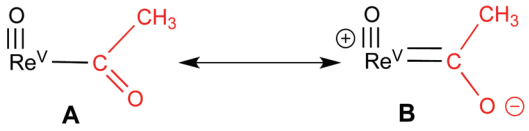

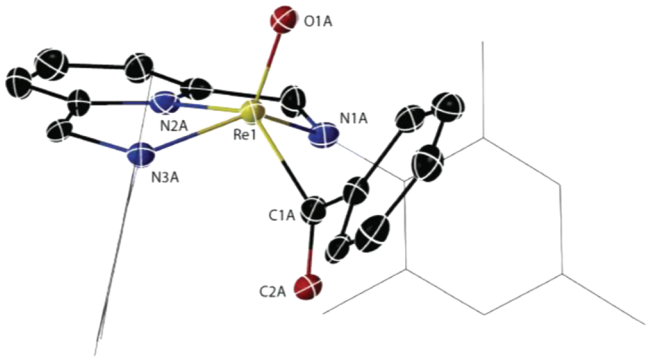

Figure 4. X-ray crystal structure of **9a**. Ellipsoids are shown at the 50% probability level. Hydrogen atoms are omitted, and the mesityl substituents on the diamido ligand are depicted in wireframe for clarity. Selected bond lengths (Å) and bond angles (deg): Re1−O1A, 1.692(4); Re1−N1A, 1.965(5); Re1−N3A, 1.983(4); Re1−N2A, 2.076(4); Re1−C1A, 2.059(6); C1A−O2A, 1.231(7); O1A−Re1−N1A, 111.43(18); O1A−Re1−N3A, 110.17(18); N1A−Re1−N3A, 137.18(18); O1A−Re1−N2A, 118.62(18); N1A−Re1−N2A, 75.63(18); N3A−Re1−N2A, 76.10(17); O1A−Re1−C1A, 104.1(2); N1A−Re1−C1A, 92.1(2); N3A−Re1−C1A, 87.3(2); N2A−Re1−C1A, 137.2(2).

dx.doi.org/10.1021/om3002872 | *Organometallics* 2012, 31, 4295−4301

The IR stretching frequency of the C(O)−Ph bond in **9a** is 1557 cm^{-1}. This IR stretch is within the range reported for other Re benzoyl complexes. For example, Sironi and co-workers reported a ν(C(O)−Ph) stretch of 1608 cm^{-1} for the dicarbonyl complex $[Cp(CO)_2Re(Me)(COPh)]$.[4a] Similarly, Djukic and co-workers reported a ν(C(O)−Ph) stretch of 1589 cm^{-1} for the rhenium benzoyl complex (benzoyl)tricarbonyl[3-methyl-2-{(η^6-phenyl)tricarbonylchromium(0)-$\kappa C2'$}pyridine-κN]rhenate(I),[12] while Gladysz and co-workers reported a ν(C(O)−Ph) stretch of 1514 cm^{-1} for the benzoyl complex $[CpRe(NO)(PPh_3)(COC_6H_5)]$.[4b] The phenyl ring in the benzoyl group rotates −45.4(7)° out of the plane in order to decrease the steric interactions between Re−O and the benzoyl group.

DFT Calculations. In order to acquire a deeper understanding of the energetics of the CO insertion reaction, DFT (B3PW91)[13] calculations were performed. All calculations were performed with the 6-31G(d,p) basis set[14] on the C, H, N, and O atoms and the SDD[15] pseudopotential and basis set augmented with an f polarization function[16] on the Re atom. As described previously, this functional and basis set accurately reproduces the geometries of related complexes.[5b] Solvation energies were calculated by applying the SMD[17] solvation model as implemented in Gaussian 09,[18] to structures optimized in the gas phase.

The results of the computational analysis are summarized in Table 1. Formations of the benzoyl complexes are the most

Table 1. Thermodynamic and Kinetic Data for the Insertion Reaction of CO with [(DAP)Re(O)(R)] Complexes

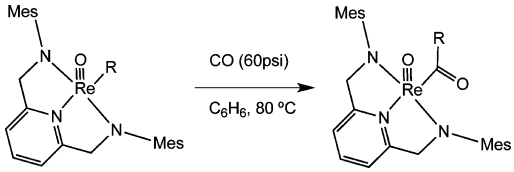

R	ΔG_{353}[a]	$\Delta G^{\ddagger}_{353}$
Me	−11.2 (−18.5)	14.6 (8.33)
p-methoxyphenyl	−16.3 (−23.5)	16.3 (21.9)
phenyl	−14.5 (−24.0)	17.4 (9.22)

[a]Solvation energies were computed geometries optimized in the gas phase (given in parentheses) using the SMD[17] method, with benzene as the solvent, as implemented in Gaussian 09.

exergonic (ΔG_{353} = −16.3 kcal/mol, R = *p*-methoxyphenyl; ΔG_{353} = −14.5 kcal/mol, R = phenyl), while formation of the acetyl complex is the least favorable (ΔG_{353} = −11.2 kcal/mol). In spite of this, formation of the acetyl complex occurs most readily (2.5 h), in comparison to 24 h for the benzoyl complexes. This suggests that the origin for the difference in reactivities is kinetic. This is also evident when the energies of activation are compared, as the formation of the acetyl complex proceeds with the lowest activation energy ($\Delta G^{\ddagger}_{353}$ = 14.6 kcal/mol), while the formation of the benzoyl complexes proceed with highesr activation energies ($\Delta G^{\ddagger}_{353}$ = 16.3 and 17.4 kcal/mol). As shown in Scheme 6, in the transition state for the insertion reaction there is a greater degree of Re−R bond cleavage in the alkyl complex (Re−CH_3 = 2.40 Å) than in the phenyl complexes (Re−Ph = 2.31 Å; Re−Ph-*p*-OMe = 2.29 Å). In addition, animation of the imaginary frequency associated with each transition state led to complete dissociation of CO and the formation of **8** or **9**. These data

Scheme 6. Geometries for Transition States for the Insertion of CO into the Re−R Bonds in 5 and 7

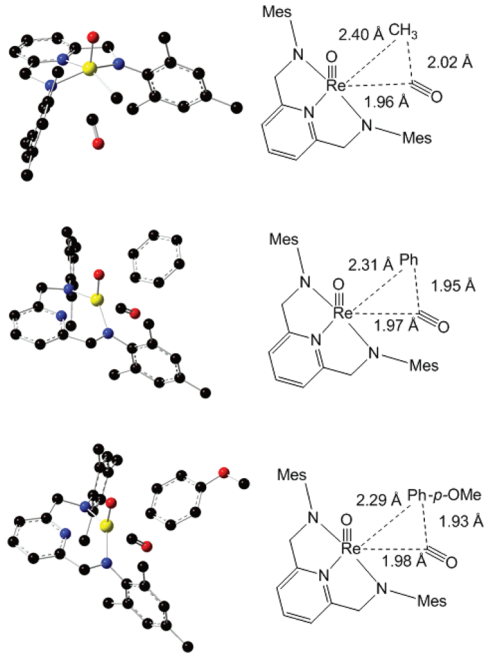

are consistent with the mechanism proposed earlier where CO inserts directly into the Re−R bond without prior formation of a CO adduct. The difference in the rate of the reactions reflects the differences in Re−R bond strengths. Recall from the X-ray crystal structures that the Re−Me bond in **5a** is 2.1278(17) Å while the Re−phenyl bond in **7a** is 2.077(2) Å. Thus, the aryl complexes react more slowly because they form stronger bonds to Re than the corresponding alkyl counterparts, and as a result, insertion of CO into these bonds is more difficult.

Conclusions. A series of oxorhenium alkyl, phenyl, and vinyl complexes of the form [(DAP)Re(O)(R)] (R = aryl, vinyl, alkyl) was reported, and their reactivity with CO was examined. The methyl complexes **5a,b** react with CO at a significantly faster rate (2.5 h) than the phenyl complexes **7** (24 h). In addition, changing the electronics of the migrating aryl ligand had no effect on the rate of insertion. Thus, it appears that the insertion of CO into the Re−R bonds in these complexes depends on the nature of the R group: i.e., aryl versus alkyl. Computational (DFT) studies reveal that although the acyl complex is the least stable (ΔG_{353} = −11.2 kcal/mol) with respect to CO insertion in comparison to the benzoyl complexes (ΔG_{353} = −16.3 and −14.5 kcal/mol), the activation energy for CO insertion is lower for the methyl complex ($\Delta G^{\ddagger}_{353}$ = 14.6 kcal/mol) than for the phenyl complexes ($\Delta G^{\ddagger}_{353}$ = 16.3 and 17.4 kcal/mol). Interestingly, unlike the case for the previously reported DAAm complexes, 1,2-migration of the acyl ligand to the oxo ligand is not observed in this system. Studies are currently being undertaken in our laboratories in order to understand the differences in reactivity between the DAAm and DAP complexes.

EXPERIMENTAL SECTION

General Considerations. 2,6-Dibromomethyl-4-methoxypyridine[9] and Re(O)Cl(DAP)[8] were prepared according to previously published procedures. All other reagents were purchased from commercial sources and used as received unless otherwise noted. THF was distilled from Na/K alloy benzophenone ketyl. ^1H and ^{13}C

dx.doi.org/10.1021/om3002872 | *Organometallics* 2012, 31, 4295−4301

NMR spectra were recorded on a Varian Mercury 400 MHz or a Varian Mercury 300 MHz spectrometer at room temperature. ^{1}H and ^{13}C NMR chemical shifts are listed in parts per million (ppm) and are referenced to residual protons and carbons of the deuterated solvents, respectively. High-pressure reactions were performed in a stainless steel Parr 4590 Micro Bench Top Reactor. FTIR spectra were obtained in KBr thin films on a JASCO FT/IR-4100 instrument. Elemental analyses were performed by Atlantic Microlabs, Inc. X-ray crystallography was performed at the X-ray Structural Facility of North Carolina State University by Dr. Paul Boyle.

2,6-Bis((mesitylamino)methyl)-4-methoxypyridine. *n*-Butyllithium (6.8 mmol, 4.25 mL) was added dropwise to a stirred solution of 2,4,6-trimethylaniline (6.8 mmol, 0.95 mL) in dry THF at −78 °C using standard Schlenk line techniques. The mixture was warmed to ambient temperature and stirred for 1 h. The reaction mixture was cooled to −78 °C, and a solution of 2,6-dibromomethyl-4-methoxypyridine (3.4 mmol, 1.0 g) in THF was added slowly. The solution was warmed to room temperature and stirred for 18 h. The mixture was quenched with a saturated $NaHCO_3$ solution (50 mL) and extracted with diethyl ether (50 mL). The organic extracts were dried over sodium sulfate and filtered. The solvent was removed under reduced pressure, resulting in a pale yellow solid (1.17 g, 42.6% yield). ^{1}H NMR ($CDCl_3$, δ): 6.86 (s, 4H, Mes *m*-H), 6.75 (s, 2H, Pyr *m*-H), 4.22 (s, 4H, MesNHCH_2), 3.82 (s, 2H, OCH_3), 2.34 (s, 12H, Mes *o*-CH_3), 2.26 (s, 6H, Mes *p*-CH_3). ^{13}C NMR ($CDCl_3$, δ): 166.95, 160.70, 143.88, 131.58, 129.99, 129.72, 106.59, 55.43, 54.29, 20.85, 18.79. HRMS (ESI): calcd for $C_{23}H_{15}F_{12}N_3$ 404.2696 [M + H$^+$], found 404.2697. Anal. Calcd: C, 51.99; N, 5.77; H, 4.71. Found: C, 51.57; N, 5.57; H, 5.03.

(4-OMeDAP)Re(O)Cl ***(4b)***. $ReOCl_3(PPh_3)_2$ (500 mg, 0.60 mmol), $(MesNHCH_2)_2NC_5H_2OMe$ (242 mg, 0.60 mmol), and 2,6-lutidine (1 mL, 8.83 mmol) were added to a 100 mL round-bottom flask with 60 mL of EtOH. The mixture was stirred at room temperature for 4 days to yield a green precipitate. The precipitate was filtered and washed with diethyl ether to give **2** (293 mg, 76.4% yield). ^{1}H NMR (CD_2Cl_2, δ): 7.27 (s, 2H, pyridine *m*-H), 6.92 (s, 2H, Mes *m*-H), 6.84 (s, 2H, Mes *m*-H), 5.52 (d, *J* = 18.0 Hz, 2H, MesNCH_2), 5.31 (d, *J* = 18.0 Hz, 2H, MesNCH_2), 4.06 (s, 3H, Pyr 4-OCH_3), 2.43 (s, 6H, Mes CH_3), 2.28 (s, 6H, Mes CH_3), 1.60 (s, 6H, Mes CH_3). ^{13}C NMR (CD_2Cl_2, δ): 171.79, 169.63, 154.57, 136.19, 134.98, 134.55, 128.79, 128.64, 103.15, 79.05, 57.21, 20.79, 18.19, 18.08. Anal. Calcd for $C_{26.25}H_{31.5}Cl_{1.5}N_3O_2Re$: C, 47.74; N: 6.63; H, 4.81. Found: C, 47.88; N, 6.45; H, 4.87.

General Procedure for Rhenium Alkyls and Phenyls. The respective Grignard reagent (0.982 mmol) was added dropwise to a solution of the respective rhenium chloride complex (0.492 mmol) in CH_2Cl_2 (15 mL) under an inert atmosphere. Water was added to the solution (25 mL), and the organic layer was extracted and dried over $NaSO_4$. The mixture was filtered, and solvent was removed under reduced pressure. The resulting residue was dissolved in a minimal amount of CH_2Cl_2, and the respective product was obtained by precipitation from excess hexanes.

(DAP)Re(O)(CH$_3$) ***(5a)***. **5a** was obtained as a red solid in 56.9% yield. ^{1}H NMR (CD_2Cl_2, δ): 8.04 (t, *J* = 7.9 Hz, 1H, NC_2H_2CH), 7.67 (d, *J* = 7.6 Hz, 2H, NC_2H_2CH), 6.92 (s, 2H, Mes *m*-H), 6.86 (s, 2H, Mes *m*-H), 5.63 (d, *J* = 22.1 Hz, 2H, MesNCH_2), 5.42 (d, *J* = 20.3 Hz, 2H, MesNCH_2), 2.39 (s, 6H, Mes CH_3), 2.28 (s, 6H, Mes CH_3), 1.76 (s, 3H, Re−CH_3), 1.53 (s, 6H, Mes CH_3). ^{13}C NMR (CD_2Cl_2, δ): 168.59, 153.59, 141.42, 136.97, 135.22, 132.41, 129.16, 129.00, 116.71, 79.47, 21.06, 18.60, 17.93, 14.60. Anal. Calcd: C, 53.04; N: 7.14; H, 5.48. Found: C, 52.86; N, 6.96; H, 5.39.

(4-OMeDAP)Re(O)CH$_3$ ***(5b)***. **5b** was obtained in 71.7% yield as a pink solid. ^{1}H NMR (CD_2Cl_2, δ): 7.14 (s, 2H, Pyr *m*-H), 6.93 (s, 2H, Mes *m*-H), 6.87 (s, 2H, Mes *m*-H), 5.56 (d, *J* = 21.0 Hz, 2H, MesNCH_2), 5.31 (d, *J* = 21.0 Hz, 2H, MesNCH_2), 4.02 (s, 3H, Pyr 4-OCH_3), 2.39 (s, 6H, Mes CH_3), 2.29 (s, 6H, Mes CH_3), 1.68 (s, 3H, Re−CH_3), 1.55 (s, 6H, Mes CH_3). ^{13}C NMR (CD_2Cl_2, δ): 169.91, 169.79, 153.42, 136.75, 134.93, 133.81, 128.81, 128.63, 102.45, 78.69, 56.78, 20.73, 18.25, 17.61, 13.44. Anal. Calcd: C, 52.41; N: 6.79; H, 5.54. Found: C, 52.00; N, 6.68; H, 5.54.

(DAP)Re(O)(CHC(CH$_3$)$_2$) ***(6)***. **6** was obtained as a brown solid in 37.8% yield. ^{1}H NMR (CD_2Cl_2, δ): 8.05 (t, *J* = 7.8 Hz, 1H, NC_2H_2CH), 7.66 (d, *J* = 7.8 Hz, 2H, NC_2H_2CH), 6.80 (s, 4H, Mes *m*-H), 6.67 (s, 1H, CH(CH_3)$_2$), 5.64 (d, *J* = 20.7 Hz, 2H, MesNCH_2), 5.37 (d, *J* = 20.7 Hz, 2H, MesNCH_2), 2.33 (s, 6H, Mes CH_3), 2.24 (s, 6H, Mes CH_3), 1.58 (s, 6H, Mes CH_3), 1.44 (s, 3H, CH(CH_3)$_2$), 1.35 (s, 3H, CH(CH_3)$_2$). ^{13}C NMR (CD_2Cl_2, δ): 168.39, 155.19, 154.81, 141.44, 136.73, 134.40, 133.85, 128.95, 128.57, 127.70, 116.91, 78.45, 27.84, 24.95, 21.03, 18.77, 18.11. Anal. Calcd for $C_{29.5}H_{37}ClN_3ORe$: C, 52.78; N: 6.26; H, 5.56. Found: C, 52.26; N, 6.11; H, 5.40.

(DAP)Re(O)(C$_6$H$_5$) ***(7a)***. **7a** was obtained as a brown solid in 67.8% yield. ^{1}H NMR (CD_2Cl_2, δ): 8.13 (t, *J* = 8.0 Hz, 1H, NC_2H_2CH), 7.74 (d, *J* = 8.0 Hz, 2H, NC_2H_2CH), 6.61 (s, 2H, Mes *m*-H), 6.57 (s, 2H, Mes *m*-H), 6.38 (dd, *J* = 6.8 Hz, 2H, Ph *m*-H), 6.18 (br, 2H, Ph *o*-H), 6.03 (t, *J* = 7.2 Hz, 1H, Ph *p*-H), 5.72 (d, *J* = 20.4 Hz, 2H, MesNCH_2), 5.54 (d, *J* = 20.4 Hz, 2H, MesNCH_2), 2.38 (s, 6H, Mes CH_3), 2.10 (s, 6H, Mes CH_3), 1.72 (s, 6H, Mes CH_3). ^{13}C NMR (CD_2Cl_2, δ): 175.49, 167.32, 153.68, 141.66, 135.88, 134.07, 133.48, 131.27, 128.48, 128.10, 125.46, 121.26, 116.88, 78.76, 20.55, 18.87, 18.08. Anal. Calcd: C, 57.21; N, 6.46; H, 5.27. Found: C, 57.02; N, 6.24; H, 5.32.

(DAP)Re(O)(C$_6$H$_4$-p-OCH$_3$) ***(7b)***. **7b** was obtained as a red solid in 59.1% yield. ^{1}H NMR (CD_2Cl_2, δ): 8.12 (t, *J* = 8.0 Hz, 1H, NC_2H_2CH), 7.73 (d, *J* = 7.6 Hz, 2H, NC_2H_2CH), 6.62 (s, 4H, Mes *m*-H), 6.05 (s, 4H, *Ph*), 5.71 (d, *J* = 20.4 Hz, 2H, MesNCH_2), 5.54 (d, *J* = 20.0 Hz, 2H, MesNCH_2), 3.45 (s, 3H, Ph OCH_3), 2.37 (s, 6H, Mes CH_3), 2.12 (s, 6H, Mes CH_3), 1.68 (s, 6H, Mes CH_3). ^{13}C NMR (CD_2Cl_2, δ): 167.44, 162.99, 156.02, 153.91, 141.63, 135.89, 134.08, 133.54, 132.17, 128.55, 128.24, 116.80, 111.76, 78.98, 55.20, 20.59, 18.86, 18.08. Anal. Calcd for $C_{32.75}H_{37.5}Cl_{1.5}N_3O_2Re$: C, 52.83; N, 5.64; H, 5.08. Found: C, 52.67; N, 5.27; H, 5.69.

(DAP)Re(O)(C$_6$H$_4$-p-Cl) ***(7c)***. **7c** was obtained as a reddish brown solid in 41.2% yield. ^{1}H NMR (CD_2Cl_2, δ): 8.15 (t, *J* = 7.6 Hz, 1H, NC_2H_2CH), 7.75 (d, *J* = 8.0 Hz, 2H, NC_2H_2CH), 6.63 (s, 2H, Mes *m*-H), 6.61 (s, 2H, Mes *m*-H), 6.35 (d, *J* = 8.0 Hz, 2H, Ph *m*-H), 6.10 (br, 2H, Ph *o*-H), 5.73 (d, *J* = 20.4 Hz, 2H, MesNCH_2), 5.55 (d, *J* = 20.0 Hz, 2H, MesNCH_2), 2.37 (s, 6H, Mes CH_3), 2.13 (s, 6H, Mes CH_3), 1.70 (s, 6H, Mes CH_3). ^{13}C NMR (CD_2Cl_2, δ): 173.52, 167.49, 153.66, 142.20, 136.03, 134.20, 132.62, 128.95, 128.47, 127.68, 125.36, 117.36, 78.85, 20.90, 19.15, 18.35. Anal. Calcd for $C_{31.5}H_{34}Cl_2N_3ORe$: C, 51.99; N, 5.77; H, 4.71. Found: C, 51.57; N, 5.57; H, 5.03.

General Procedure for CO Insertions. The respective rhenium complex (0.308 mmol) was placed in a 50 mL glass-lined Parr reactor and dissolved in benzene (10 mL). The reactor was purged and pressurized with CO (200 psi). The reaction mixture was heated to 80 °C and stirred for either 2.5 h (methyl complexes) or 24 h (phenyl complexes). The mixture was cooled to room temperature, and the solvent was removed under reduced pressure. The resulting residue was dissolved in a minimal amount of CH_2Cl_2, and the respective product was precipitated out by the addition of excess hexanes.

(DAP)Re(O)(COCH$_3$) ***(8a)***. **8a** was obtained as an orange solid in 57.8% yield. ^{1}H NMR (CD_2Cl_2, δ): 8.08 (t, *J* = 7.6 Hz, 1H, NC_2H_2CH), 7.67 (d, *J* = 7.6 Hz, 2H, NC_2H_2CH), 6.85 (s, 2H, Mes *m*-H), 6.80 (s, 2H, Mes *m*-H), 5.65 (d, *J* = 21.0 Hz, 2H, MesNCH_2), 5.44 (d, *J* = 21.0 Hz, 2H, MesNCH_2), 2.48 (s, 6H, Mes CH_3), 2.26 (s, 6H, Mes CH_3), 1.88 (s, 6H, Mes CH_3), 1.78 (s, 3H, Re−COCH_3). ^{13}C NMR (CD_2Cl_2, δ): 259.1, 167.61, 154.08, 141.52, 136.38, 135.96, 134.71, 129.00, 128.61, 117.68, 75.69, 47.99, 21.05, 18.49, 18.42. Anal. Calcd for $C_{28}H_{34}Cl_2N_3O_2Re$: C, 47.93; N, 5.99; H, 4.88. Found: C, 48.21; N, 5.92; H, 4.78. IR (FTIR, cm^{-1}): ν(C−O) 1599 cm^{-1}.

(4-OMeDAP)Re(O)(COCH$_3$) ***(8b)***. In a J. Young tube **5b** (4.1 mg, 0.0066 mmol) was dissolved in CD_2Cl_2, and CO (60 psi) was added via three freeze−pump−thaw cycles. Product formation was observed by ^{1}H NMR spectroscopy. ^{1}H NMR (CD_2Cl_2, δ): 7.09 (s, 2H, pyridine *m*-H), 6.82 (s, 2H, Mes *m*-H), 6.78 (s, 2H, Mes *m*-H), 5.54 (d, *J* = 19.9 Hz, 2H, MesNCH_2), 5.29 (d, *J* = 21.0 Hz, 2H, MesNCH_2), 4.00 (s, 3H, Pyr 4-OCH_3), 2.44 (s, 6H, Mes CH_3), 2.25 (s, 6H, Mes CH_3), 1.86 (s, 6H, Mes CH_3), 1.73 (s, 3H, Re−COCH_3).

(DAP)Re(O)(COC$_6$H$_5$) ***(9a)***. **9a** was obtained in 55.6% yield as an orange solid. ^{1}H NMR (CD_2Cl_2, δ): 8.14 (t, *J* = 7.8 Hz, 1H, NC_2H_2CH), 7.70 (d, *J* = 7.8 Hz, 2H, NC_2H_2CH), 7.16 (t, *J* = 8.1 Hz,

Table 2. Selected Crystallographic Data and Collection Parameters for (DAP)Re(O)(CHC(CH$_3$)$_2$) (6), (DAP)Re(O)(C$_6$H$_5$) (7a), (DAP)Re(O)(COCH$_3$) (8a), and (DAP)Re(O)(COC$_6$H$_5$) (9a)

	6	7a	8a	9a
empirical formula	$C_{28.85}H_{35.74}Br_{0.04}N_3ORe$	$C_{31}H_{34}N_3ORe$	$C_{28}H_{34}C_{12}N_3O_2Re$	$C_{32}H_{34}N_3O_2Re$
formula wt	629.75	650.81	701.68	678.82
cryst dimens/mm	0.41 × 0.10 × 0.03	0.19 × 0.17 × 0.13	0.16 × 0.14 × 0.05	0.08 × 0.08 × 0.01
cryst syst	monoclinic	monoclinic	monoclinic	triclinic
space group	$P2_1/c$	$P2_1/c$	$P2_1/c$	$P\bar{1}$
a/Å	16.998(5)	17.067(6)	7.9735(6)	13.536(5)
b/Å	18.682(5)	16.635(7)	13.8238(10)	13.995(4)
c/Å	20.185(7)	18.941(7)	25.7538(18)	15.660(6)
α (deg)	90.00	90.00	90.00	78.110(18)
β (deg)	124.049(7)	92.891(12)	95.107(4)	79.25(2)
γ (deg)	90.00	90.00	90.00	75.795(18)
V/Å^3	5311(3)	5371(3)	2827.4(4)	2785.0(17)
Z	8	8	4	4
ρ/g cm^{-3}	1.575	1.610	1.648	1.619
R1, wR2($I > 2\sigma(I)$)	0.0356, 0.0677	0.0331, 0.0571	0.0390, 0.0750	0.0429, 0.724
GOF	1.024	1.036	1.028	1.003

1H, Ph *p*-H), 7.04 (dd, J = 8.1 Hz 2H, Ph *m*-H), 6.82 (d, J = 7.2 Hz, 2H, Ph *o*-H), 6.75 (s, 2H, Mes *m*-H), 6.53 (s, 2H, Mes *m*-H), 5.70 (d, J = 20.7 Hz, 2H, MesNCH_2), 5.49 (d, J = 20.4 Hz, 2H, MesNCH_2), 2.18 (s, 6H, Mes CH_3), 2.17 (s, 6H, Mes CH_3), 1.96 (s, 6H, Mes CH_3). ^{13}C NMR (CD_2Cl_2, δ): 262.02, 167.63, 154.16, 147.57, 141.74, 136.44, 136.10, 134.57, 130.28, 128.79, 128.31, 127.56, 126.72, 117.74, 75.85, 20.91, 18.62, 18.28. Anal. Calcd: C, 56.62; N: 6.19; H, 5.05. Found: C, 56.40; N, 6.19; H, 5.08. IR (FTIR, cm^{-1}): ν(C−O) 1557 cm^{-1}.

*(DAP)Re(O)(COC$_6$H$_4$-p-OCH$_3$) (**9b**).* **9b** was obtained in 63.6% yield as an orange solid. ^{1}H NMR (CD_2Cl_2, δ): 8.13 (t, J = 8.0 Hz, 1H, NC$_2$H$_2$C*H*), 7.69 (d, J = 8.0 Hz, 2H, NC$_2$H$_2$CH), 6.86 (d, J = 9.2 Hz, 2H, Ph H), 6.74 (s, 2H, Mes *m*-H), 6.56 (d, J = 8.8 Hz, 2H, Ph H), 6.52 (s, 2H, Mes *m*-H), 5.69 (d, J = 20.4 Hz, 2H, MesNCH_2), 5.49 (d, J = 20.8 Hz, 2H, MesNCH_2), 3.74 (s, 3H, Ph OCH_3), 2.18 (s, 6H, Mes CH_3), 2.16 (s, 6H, Mes CH_3), 1.94 (s, 6H, Mes CH_3). ^{13}C NMR (CD_2Cl_2, δ): 260.55, 167.70, 161.76, 154.19, 141.68, 139.97, 136.45, 136.05, 134.41, 128.71, 128.67, 128.28, 117.70, 112.71, 75.94, 55.69, 20.91, 18.64, 18.34. Anal. Calcd: C, 55.91; N, 5.93; H, 5.12. Found: C, 55.10; N, 6.32; H, 5.31. IR (FTIR, cm^{-1}): ν(C−O) 1552 cm^{-1}.

*(DAP)Re(O)(COC$_6$H$_4$-p-Cl) (**9c**).* **9c** was obtained in 52.7% yield as an orange solid. ^{1}H NMR (CD_2Cl_2, δ): 8.14 (t, J = 7.6 Hz, 1H, NC$_2$H$_2$C*H*), 7.70 (d, J = 8.0 Hz, 2H, NC$_2$H$_2$CH), 7.02 (d, J = 8.4 Hz, 2H, Ph H), 6.80 (d, J = 8.4 Hz, 2H, Ph H), 6.74 (s, 2H, Mes *m*-H), 6.54 (s, 2H, Mes *m*-H), 5.71 (d, J = 21.2 Hz, 2H, MesNCH_2), 5.50 (d, J = 20.4 Hz, 2H, MesNCH_2), 2.18 (s, 6H, Mes CH_3), 2.17 (s, 6H, Mes CH_3), 1.94 (s, 6H, Mes CH_3). ^{13}C NMR (CD_2Cl_2, δ): 260.62, 167.58, 154.07, 145.93, 141.88, 136.40, 136.11, 135.99, 134.70, 128.84, 128.30, 128.15, 127.72, 117.85, 75.77, 20.91, 18.60, 18.28. Anal. Calcd for $C_{32.5}H_{34}Cl_2N_3O_2Re$: C, 51.65; N, 5.56; H, 4.53. Found: C, 51.08; N, 5.55; H, 4.68. IR (FTIR, cm^{-1}): ν(C−O) 1554 cm^{-1}.

General Procedure for X-ray Determination. The sample was mounted on a Mitegen polyimide micromount with a small amount of Paratone N oil. All X-ray measurements were carried out on a Bruker-Nonius Kappa Axis X8 Apex2 diffractometer at a temperature of 110 K. The frame integration was performed using SAINT.[19] Unless otherwise noted, the resulting raw data were scaled and absorption-corrected using a multiscan averaging of symmetry equivalent data using SADABS.[20] The structural model was fit to the data using full-matrix least squares based on F^2. The calculated structure factors included corrections for anomalous dispersion from the usual tabulation. The structure was refined using the XL program from SHELXTL;[21] graphic plots were produced using the NRCVAX crystallographic program suite. Additional information and other relevant literature references can be found in the reference section of the Facility's Web page (http://www.xray.ncsu.edu).

*X-ray Structural Determination of (DAP)Re(O)(CHC(CH$_3$)$_2$) (**6**).* The unit cell dimensions were determined from a symmetry-constrained fit of 9300 reflections with 5.0° < 2θ < 64.76°. The data collection strategy was a number of ω and φ scans which collected data up to 79.48° (2θ). The structure was solved by direct methods using the XS program.[22] All non-hydrogen atoms were obtained from the initial solution. The hydrogen atoms were introduced at idealized positions and were allowed to ride on the parent atom. The structure contains two molecules in the asymmetric unit, designated **A** and **B** in this report. The structure also exhibits a compositional disorder with the bromo derivative of the complex cocrystallizing at the same site as molecule **A**. The normalized occupancy of the bromine atom refined to a value of 0.075(2). The assignment of the Br atom was inferred by the Re−X bond length of 2.509(6) Å in comparison to the Re−Br bond lengths of other Re−oxo bromide compounds recovered from a CSD search. *Note*: the final difference Fourier map showed a number of large peaks. However, these peaks were in chemically unreasonable positions or could not be refined reasonably. It cannot be said for sure what the origin of these peaks are. See Table 2.

*X-ray Structural Determination of (DAP)Re(O)(C$_6$H$_5$) (**7a**).* The unit cell dimensions were determined from a symmetry-constrained fit of 9482 reflections with 4.9° < 2θ < 65.28°. The data collection strategy was a number of ω and φ scans which collected data up to 75.66° (2θ). The structure was solved by direct methods using the XS program.[22] All non-hydrogen atoms were obtained from the initial solution. The hydrogen atoms were introduced at idealized positions and were allowed to ride on the parent atom. The final difference Fourier map contains a region of large positive residual region of electron density (3.17 e/Å^3). An attempt was made to model this site both as an oxygen and as a lithium, but in both cases the displacement parameter refined to a large value which was incongruent with the rest of the structure. The behavior of the refinement as well as the fact that there is no analogous peak close to the B molecule and the peak is not at a chemically sensible position led to the conclusion that this peak is an artifact rather than an indicator of actual atomic electron density. See Table 2.

*X-ray Structural Determination of (DAP)Re(O)(COCH$_3$) (**8a**).* The unit cell dimensions were determined from a symmetry-constrained fit of 9918 reflections with 5.6° < 2θ < 58.58°. The data collection strategy was a number of ω and φ scans which collected data up to 65.22° (2θ). The structure was solved by direct methods using the SIR92 program.[23] Most non-hydrogen atoms were obtained from the initial solution. The remaining non-hydrogen atom positions were obtained from a subsequent difference Fourier map. The hydrogen atoms were introduced at idealized positions and were allowed to ride on the parent atom. See Table 2.

dx.doi.org/10.1021/om3002872 | *Organometallics* 2012, 31, 4295−4301

*X-ray Structural Determination of (DAP)Re(O)(COC_6H_5) (**9a**).* The unit cell dimensions were determined from a symmetry-constrained fit of 9995 reflections with 5.8° < 2θ < 63.48°. The data collection strategy was a number of ω and φ scans which collected data up to 64.62° (2θ). The structure was solved by direct methods using the XS program.[22] All non-hydrogen atoms were obtained from the initial solution. The hydrogen atoms were introduced at idealized positions and were allowed to ride on the parent atom. See Table 2.

Computational Methods. Theoretical calculations were carried out using the Gaussian09[18] implementation of B3PW91 (the B3 exchange functional[13a] and PW91 correlation functional[13b]) density functional theory.[13c] All geometry optimizations were carried out using tight convergence criteria ("opt=tight") and pruned ultrafine grids ("Int=ultrafine"). All calculations were conducted with the same basis set combination. The basis set for rhenium was the small-core (311111,22111,411) → [6s5p3d] Stuttgart–Dresden basis set and relativistic effective core potential (RECP) combination (SDD)[15] with an additional f polarization function.[16] The 6-31G(d,p)[14] basis sets were used for all other atoms. Cartesian d functions were used throughout; i.e., there are six angular basis functions per d function. All structures were fully optimized, and analytical frequency calculations were performed on all structures to ensure either a zeroth-order saddle point (a local minimum) or a first-order saddle point (transition state TS) was achieved. The minimum associated with each transition state was determined by animation of the imaginary frequency and, if necessary, with intrinsic reaction coordinate (IRC) calculations. Solvation energies were computed geometries optimized in the gas phase using the SMD[17] method, with benzene as the solvent, as implemented in Gaussian 09. In this method an IEFPCM[24] calculation is performed with radii and electrostatic terms from Truhlar and co-workers' SMD[17] solvation model. Thermochemical data were calculated using unscaled vibrational frequencies and default parameters at 353.15 K and 1 atm. In this paper energies are reported in kcal/mol with gas-phase energies in parentheses and solvation energies without parentheses.

■ ASSOCIATED CONTENT

Supporting Information

Tables giving Cartesian coordinates and figures giving the structures for all optimized complexes, text giving the full Gaussian 09 reference, a figure giving the time profile for CO insertion into **5** and **7**, and CIF files giving crystal data for **6**, **7a**, **8a**, and **9a**. This material is available free of charge via the Internet at http://pubs.acs.org.

■ AUTHOR INFORMATION

Corresponding Author

*E-mail: eaison@ncsu.edu.

Notes

The authors declare no competing financial interest.

■ ACKNOWLEDGMENTS

We acknowledge North Carolina State University and the National Science Foundation via the CAREER Award (CHE-0955636) for funding.

■ REFERENCES

(1) (a) Zoeller, J. R.; Agreda, V. H.; Cook, S. L.; Lafferty, N. L.; Polichnowski, S. W.; Pond, D. M. *Catal. Today* **1992**, *13*, 73–91. (b) Zoeller, J. R. *Catal. Today* **2009**, *140*, 118–126. (c) van Leeuwen, P. W. N. M.; Freixa, Z. In *Carbon Monoxide As a Chemical Feedstock: Carbonylation Catalysis*; Wiley-VCH: Weinheim, Germany, 2006; pp 319–356. (d) Haynes, A. *Adv. Catal.* **2010**, *53*, 1–45. (e) Haynes, A. *Top. Organomet. Chem.* **2006**, *18*, 179–205. (f) Cheong, M.; Ziegler, T. *Organometallics* **2005**, *24*, 3053–3058.

(2) Ojima, I.; Tsai, C.-Y.; Tzamarioudaki, M.; Bonafoux, D. *The Hydroformylation Reaction*; Wiley: New York, 2004.

(3) (a) Chaplin, A. B.; Hooper, J. F.; Weller, A. S.; Willis, M. C. *J. Am. Chem. Soc.* **2012**, *134*, 4885–4897. (b) Meng, Q.; Shen, W.; Li, M. *J Mol Model* **2012**, *18*, 1229–39. (c) Willis, M. C. *Chem Rev* **2010**, *110*, 725–748.

(4) (a) Bergamo, M.; Beringhelli, T.; D'Alfonso, G.; Maggioni, D.; Mercandelli, P.; Sironi, A. *Inorg. Chim. Acta* **2003**, *350*, 475–485. (b) Buhro, W. E.; Wong, A.; Merrifield, J. H.; Lin, G. Y.; Constable, A. C.; Gladysz, J. A. *Organometallics* **1983**, *2*, 1852–1859. (c) Liu, J.; Heaton, B. T.; Iggo, J. A.; Whyman, R. *Chem. Commun.* **2004**, 1326–1327.

(5) (a) Smeltz, J. L.; Boyle, P. D.; Ison, E. A. *J. Am. Chem. Soc.* **2011**, *133*, 13288–13291. (b) Smeltz, J. L.; Webster, C. E.; Ison, E. A. *Organometallics* **2012**, DOI: 10.1021/om3003366.

(6) (a) Alt, H. G.; Hayen, H. I. *Angew. Chem., Int. Ed. Engl.* **1985**, *24*, 497–498. (b) Antinolo, A.; del, H. I.; Lopez-Solera, I.; Garcia-Yuste, S.; Otero, A.; Fajardo, M.; Rodriguez, A. *J. Organomet. Chem.* **2000**, *598*, 167–173. (c) Cai, S.; Hoffman, D. M.; Lappas, D.; Woo, H. G.; Huffman, J. C. *Organometallics* **1987**, *6*, 2273–2278. (d) Hoffman, D. M.; Lappas, D.; Wierda, D. A. *Polyhedron* **1996**, *15*, 3309–3314.

(7) (a) Feng, S. G.; Luan, L.; White, P.; Brookhart, M. S.; Templeton, J. L.; Young, C. G. *Inorg. Chem.* **1991**, *30*, 2582–2584. (b) Malarek, M. S.; Evans, D. J.; Smith, P. D.; Bleeker, A. R.; White, J. M.; Young, C. G. *Inorg. Chem.* **2006**, *45*, 2209–2216. (c) Su, F. M.; Cooper, C.; Geib, S. J.; Rheingold, A. L.; Mayer, J. M. *J. Am. Chem. Soc.* **1986**, *108*, 3545–3547. (d) Cross, J. L.; Crane, T. W.; White, P. S.; Templeton, J. L. *Organometallics* **2003**, *22*, 548–554.

(8) Lilly, C. P.; Boyle, P. D.; Ison, E. A. *Dalton Trans.* **2011**, *40*, 11815–11821.

(9) Pellegatti, L.; Zhang, J.; Drahos, B.; Villette, S.; Suzenet, F.; Guillaumet, G.; Petoud, S.; Toth, E. *Chem. Commun.* **2008**, 6591–3.

(10) Bodner, G. S.; Patton, A. T.; Smith, D. E.; Georgiou, S.; Tam, W.; Wong, W. K.; Strouse, C. E.; Gladysz, J. A. *Organometallics* **1987**, *6*, 1954–1961.

(11) Goldberg, K. I.; Bergman, R. G. *J. Am. Chem. Soc.* **1989**, *111*, 1285–1299.

(12) (a) Djukic, J.-P.; Maisse, A.; Pfeffer, M.; Dötz, K. H.; Nieger, M. *Organometallics* **1999**, *18*, 2786–2790. (b) Djukic, J.-P.; Doetz, K. H.; Pfeffer, M.; De, C. A.; Fischer, J. *Inorg. Chem.* **1998**, *37*, 3649–3651.

(13) (a) Becke, A. D. *J. Chem. Phys.* **1993**, *98*, 5648–52. (b) Perdew, J. P.; Chevary, J. A.; Vosko, S. H.; Jackson, K. A.; Pederson, M. R.; Singh, D. J.; Fiolhais, C. *Phys. Rev. B: Condens. Matter* **1992**, *46*, 6671–87. (c) Parr, R. G., Yang, W. *Density Functional Theory of Atoms and Molecules*; Oxford University Press: New York, 1989.

(14) Hehre, W. J.; Ditchfield, R.; Pople, J. A. *J. Chem. Phys.* **1972**, *56*, 2257–61.

(15) Dolg, M.; Stoll, H.; Preuss, H.; Pitzer, R. M. *J. Phys. Chem.* **1993**, *97*, 5852–9.

(16) Ehlers, A. W.; Boehme, M.; Dapprich, S.; Gobbi, A.; Hoellwarth, A.; Jonas, V.; Koehler, K. F.; Stegmann, R.; Veldkamp, A.; et al. *Chem. Phys. Lett.* **1993**, *208*, 111–14.

(17) Marenich, A. V.; Cramer, C. J.; Truhlar, D. G. *J. Phys. Chem. B* **2009**, *113*, 6378–6396.

(18) Frisch, M. J.; Trucks, G. W.; Schlegel, H. B. et al. *Gaussian 09, Revision A.02*; Gaussian, Inc., Wallingford, CT, 2009.

(19) *SAINT version 2009.9*; Bruker-Nonius, Madison, WI 53711, 2009.

(20) *SADABS version 2009.9*; Bruker-Nonius, Madison, WI 53711, 2009.

(21) *XL version 2009.9*; Bruker-Nonius, Madison, WI 53711, 2009.

(22) *XS version 2009.9*; Bruker-Nonius, Madison, WI 53711, 2009.

(23) Altomare, A.; Cascarano, G.; Giacovazzo, C.; Guagliardi, A.; Burla, M. C.; Polidori, G.; Camalli, M. *J. Appl. Crystallogr.* **1994**, *27*, 435–436.

(24) Tomasi, J.; Mennucci, B.; Cammi, R. *Chem. Rev.* **2005**, *105*, 2999–3093.